Small-molecule control of antibody N-glycosylation in engineered mammalian cells

Precise control of N-linked glycosylation of a recombinant antibody in genetically engineered mammalian cells

Michelle M. Chang, Leonid Gaidukov, Giyoung Jung, Wen Allen Tseng, John J. Scarcelli, Richard Cornell, Jeffrey K. Marshall, Jonathan L. Lyles, Paul Sakorafas, An-Hsiang Adam Chu, Kaffa Cote, Boriana Tzvetkova, Sepideh Dolatshahi, Madhuresh Sumit, Bhanu Chandra Mulukutla, Douglas A. Lauffenburger, Bruno Figueroa, Nevin M. Summers, Timothy K. Lu, Ron Weiss

Abstract

N-linked glycosylation in monoclonal antibodies (mAbs) is crucial for the structural and functional properties of mAb therapeutics, such as conformational and thermal stability, pharmacokinetics and pharmacodynamics, safety, and clinical efficacy. However, the biopharmaceutical industry lacks the tools to precisely control or dictate N-glycosylation levels during mAb production. In this study, we engineered CHO cells with synthetic genetic circuits in order to precisely tune the N-glycosylation pattern of a stably expressed IgG. We knocked out two key glycosyltransferase genes, α-1,6-fucosyltransferase (*FUT8*) and β-1,4-galactosyltransferase (*β4GALT1*) in order to eliminate endogenous fucosylation and galactosylation. Then, we used genetic circuits expressing synthetic copies of *FUT8* and *β4GALT1* under constitutive or inducible promoters to generate antibodies with concurrently desired fucosylation (0-97%) and galactosylation (0-87%) levels. This precise fine-tuning of glycosylation was enabled through the simultaneous and independent control of *FUT8* and *β4GALT1* expression using two orthogonal small molecule inducers. Effector function studies

confirmed that changing the glycosylation profile impacted antibody binding to a cell surface receptor. Precise and rational modification of glycosylation patterns of recombinant proteins will allow new protein therapeutics to have tailored in vitro and in vivo effects for various biotechnological and biomedical applications.

Introduction

Monoclonal antibodies (mAbs) are currently used in a wide variety of therapeutic applications, including the treatment of several cancers and autoimmune diseases.[1–3] The solubility, stability, folding accuracy, pharmacokinetics, and biological activity of mAb therapeutics are heavily dependent upon their N-linked glycosylation at Asn297 in the Fc region of IgG antibodies.[4–7] The diversity and complexity of these N-glycans can be attributed to the high number of different sugar moieties and the multitude of possible linkages, with different glycan structures yielding distinct biological functions. For example, mannosylated and sialylated glycans impact pharmacokinetics.[4] Fucosylation strongly affects IgG binding to Fcγ receptors and thereby influences antibody-dependent cell-mediated cytotoxicity (ADCC)[8] and antibody-dependent cell-mediated phagocytosis (ADCP),[9] while galactosylation is important for complement-dependent cytotoxicity (CDC).[10] In addition, glycans can affect mAb safety, as immunogenicity can be a problem when mAbs are produced in cell lines that make certain sugars or linkages not naturally present in humans. Furthermore, due to the incomplete modification of glycans at each step along the N-glycan processing pathway, existing antibody therapeutics are typically heterogeneous mixtures of glycoforms. Since different glycoforms may differ in biological activity, consistency of this glycosylation heterogeneity is expected.[7] Thus, control of the glycosylation profiles is essential for biopharmaceutical production.

As a result of the influence that these different glycoforms have on function, there has been increased interest in glycoengineering antibodies to obtain products with distinct N- glycan structures.[4,7,11,12] Current glycoengineering efforts mostly rely on manipulating culture conditions, generating knockouts, and transient expression of IgG and glycan remodeling enzymes.[13] One strategy focuses on in-process controls such as culture temperature, pH, and feed.[14] In one such study, media modification increased antibody galactosylation in GS-CHO cells from 3% to 23% in bioreactors.[15] Another strategy targets certain genes for disruption. For example, RNA interference has been used against α-1,6-fucosyltransferase *(FUT8)* gene expression to reduce fucosylation.[16] Afucosylation has been achieved by knocking out *FUT8* or the enzymes responsible for biosynthesis of GDP-fucose.[17–22] In addition, knockouts of many glycosyltransferase genes along the N-glycosylation pathway have been made in HEK293S and CHO-K1 cells in efforts to reduce heterogeneity.[23,24] Another approach is transient overexpression of glycosyltransferase genes, such as β-1,4-galactosyltransferase *(β4GALT1)* and β-galactosidase α-2,6-sialyltransferase *(ST6GAL1)* genes, to enrich mAb galactosylation and sialylation, respectively.[12,25] Transient overexpression can be used to achieve different levels of glycosylation, but each desired level requires a co-transfection with different amounts of DNA encoding the glycosyltransferases,[12] and this method would be costly to scale up for industrial production. In vitro enzymatic glycoengineering of purified mAbs results in finer control of glycosylation levels when compared with current in vivo methods, but requires additional purification steps and is also not easily scalable.

Existing glycoengineering methods allow either modest changes, such as in the case of media supplementation, or all-or-nothing changes in the case endogenous gene deletion and overexpression of synthetic genes. Ideally, precise control of enzymatic activity would permit

specific control of glycosylation levels. This would enable engineering and testing of new antibody therapeutics or improvement of existing ones. Here, we engineered suspension CHO cells to express an IgG1 antibody (called mAb), used as a functional readout for glycosylation, and deleted two key endogenous glycosyltransferase genes, *FUT8* and *β4GALT1*, which control mAb fucosylation and galactosylation (Fig. 1). We then introduced genetic circuits expressing synthetic versions of *FUT8* and *β4GALT1* under various constitutive and inducible promoters. Through simultaneous and independent induction with doxycycline and abscisic acid, we achieved precise fine-tuning of fucosylation (0-95%) and galactosylation (0-87%). Because Fc fucosylation and galactosylation levels directly influence effector functions, independent control of both is desired. Typical mAbs are highly fucosylated but only have low levels of galactosylation. Intermediate glycosylation levels are useful for probing the biological properties and effector function capabilities of mAbs with variable N-glycan profiles or for recapitulating the levels in existing mAb therapeutics to create biosimilars. Overall, our genetically engineered platform can be applied to any recombinant protein for the precise, comprehensive control and rational modification of its glycosylation profile and the subsequent biological activity.

Results

Generation of FUT8$^{-/-}$ and β4GALT1$^{-/-}$ cells expressing mAb

We based our cell-line engineering efforts on a new multi-landing pad (LP) DNA integration platform which allows for robust long-term expression of DNA payloads from stable genomic loci.[26] Protein producing cell lines generated with random integration using dihydrofolate reductase and glutamine synthetase expression selection systems yield cell lines with a wide range of expression, growth, and stability characteristics, including unstable or

93 silenced transgene expression.[27–29] While direct integration into site-specific loci mediated by
94 CRISPR/Cas9 and homology-directed DNA repair pathway can be used, the frequency of
95 homologous recombination decreases as the size of the inserted heterologous DNA increases.[30]
96 Instead, we used the multi-LP platform to engineer suspension serum-free CHO cells that bore
97 multiple landing pads for stable expression of mAb and different genetic circuits encoding
98 synthetic versions of *FUT8* and *β4GALT1* genes (Fig. 1). Using multi-LP cell lines for the
99 integration of mAb payloads and large genetic circuits into pre-selected loci enables control of
100 the integration sites and gene copy number of the payloads, thus resulting in long-term stable and
101 consistent expression levels.

102 First, we used CRISPR/Cas9 to construct multi-landing pad cell lines by inserting a
103 recombination site and a selectable marker into genomic loci that were previously identified as
104 stable integration sites in CHO (Supplementary Fig. 1).[26,31] Then, a matching site-specific
105 recombinase was used to insert a DNA payload specifically into that locus. Two or three
106 orthogonal recombination sites with different fluorescent reporters and antibiotic selection
107 markers were used to target payload integration into specific landing pad sites in multi-LP cell
108 lines. For the double landing pad (dLP) cell line, the first landing pad in the LP2 locus was
109 integrated with a payload encoding two mAb copies, and the second landing pad (LP20) was
110 available for integration with synthetic gene circuits. For the triple landing pad (tLP) cell line,
111 the third landing pad (LP8) was additionally available for integration of synthetic circuits. The
112 mAb payload was integrated first and serves as a wild-type (WT) control of endogenous levels of
113 glycosylation before knockouts and subsequent glycan profile modulations were generated.

114 Next, we eliminated endogenous Fut8 and β4GalT1 activity so that the synthetic gene
115 circuits integrated in the landing pads would exclusively control glycosylation levels. *FUT8* and

116 *β4GALT1* functional knockouts were generated in mAb expressing CHO cell lines using
117 CRISPR/Cas9 targeted excision of exons within the catalytic domains of the glycosyltransferases
118 (Fig. 1, Supplementary Fig. 2).[20,32] *FUT8*$^{-/-}$ and *β4GALT1*$^{-/-}$ clones were identified with a PCR
119 screen of genomic DNA. We isolated the mAb using Protein A purification, then enzymatically
120 released and labeled mAb glycans from each putative knockout were analyzed by hydrophilic
121 interaction liquid chromatography (HILIC) and demonstrated the loss of fucosylated and/or
122 galactosylated species (Fig. 2). As expected, when compared to the parental mAb expressing
123 CHO cell line with no gene deletions, the *FUT8*$^{-/-}$ clone exhibited conversion of G1F and G0F,
124 two fucosylated biantennary complex glycan species, to G1 and G0 species lacking fucose. The
125 *β4GALT1*$^{-/-}$ clone exhibited conversion of G1F, a monogalactosylated species, to a G0F species
126 lacking galactose. The *FUT8*$^{-/-}$*/β4GALT1*$^{-/-}$ clone exhibited conversion of G0F and G1F species
127 to a G0 species lacking both fucose and galactose, with increases in Man5 and G0-N species.
128
129 *Constitutive FUT8 and β4GALT1 expression results in high fucosylation or high galactosylation*
130 After deleting endogenous *FUT8* and *β4GALT1* genes and eliminating fucosylation and
131 galactosylation activity, we introduced synthetic versions of *FUT8* and *β4GALT1* (coding
132 sequence only) to complement our knockouts and restore activity. Expression of *FUT8* and
133 *β4GALT1* synthetic genes using the human elongation factor 1 alpha (hEF1a) promoter, a strong
134 constitutive mammalian promoter, resulted in high fucosylation and galactosylation levels.
135 Circuit FUT8-C, encoding *FUT8* gene under the hEF1a promoter and a fluorescent reporter
136 mKate, was integrated into LP20 of the *FUT8*$^{-/-}$ cell line (Fig. 3a). The puromycin resistance
137 marker and the mKate fluorescent marker were used in selection and sorting of the integrated
138 cells to select a homogeneous population of integrants expressing circuit FUT8-C. Pooled circuit

FUT8-C integrants in *FUT8*$^{-/-}$ cells had total fucosylation of mAb restored to 92.7%, similar to the wild-type levels observed in CHO cells expressing endogenous *FUT8* (Fig. 3b, Table 1). A small increase in the levels of galactosylated species was also seen. Similarly, circuit B4GALT1-C, encoding *β4GALT1* under the hEF1a promoter and a fluorescent reporter, was integrated into LP20 of the *β4GALT1*$^{-/-}$ cell line, which resulted in 87.1% total galactosylated species, a large increase from the 6.9% total galactosylated species found in *β4GALT1* wild-type cells expressing mAb. Due to the significant increase in the galactosylation levels, the percentage of sialylated species increased from 0.3% to 6.8%. Terminal galactosylation is a prerequisite for sialylation, which has been implicated in important anti-inflammatory activities.[33,34] High galactosylation levels are desirable for increased complement-dependent cytotoxicity, while low fucosylation levels are desirable for increased antibody-dependent cell-mediated cytotoxicity. Overall, we were able to replace deleted endogenous genes with the synthetic genes integrated into the LPs and to restore or enhance the glycosylation phenotype in the knockout strains. These results demonstrated the suitability of our genetically engineered cells for rational modulation of the glycosylation profile.

FUT8 or β4GALT1 single gene expression is regulated with inducible promoters

Constitutive overexpression of exogenous *FUT8* and *β4GALT1* is an important step towards accomplishing large-scale modification of mAb glycosylation profiles. Specifically, we were able to achieve high levels of fucosylation and galactosylation using the hEF1a constitutive promoter. However, the ability to fine tune fucosylation or galactosylation levels is desirable in order to study how specific glycosylation profiles affect the biological function of antibodies. Existing mAb therapeutics have been produced with their native N-glycan profiles, but

modulating the glycosylation to newly attainable levels would allow for a more extensive correlation of mAb biological functions with varied proportions of each biantennary complex glycan structures. Antibodies with high galactosylation and low fucosylation have strong ADCC effector function properties, and we were able to attain these levels in a controllable manner with synthetic *FUT8* and *β4GALT1* genes expressed under small molecule inducible promoters (Fig. 4).

In order to achieve tunable expression, we created circuits FUT8-Dox and B4GALT1-Dox that employ the Tet-On rtTA3 (reverse tetracycline transactivator) system, in which rtTA3 binds to the TRE-Tight promoter in the presence of doxycycline (Dox) and induces gene expression (Fig. 4a).[35] Dox-inducible circuits for regulating *FUT8* and *β4GALT1* expression were integrated into LP20 of the *FUT8* or *β4GALT1* single knockout cell lines. With circuit FUT8-Dox, fucosylation levels ranged from 9.3% (leaky expression without induction) to 94.0% under the highest induction levels (0-3 uM Dox) (Fig. 4b, Table 1). With circuit B4GALT1-Dox, total galactosylation levels ranged from 3.0% to 78.1% (Fig. 4c, Table 1). Intermediate glycosylation levels could be achieved by varying the induction conditions using various Dox concentrations. The highest fucosylation and galactosylation levels possible with the Dox-inducible systems are almost as high as the constitutively expressed *FUT8* or *β4GALT1* levels.

A second inducible system was needed for independent inducible control of two enzymes at once. Designed to be orthogonal to the Dox-inducible system, we created circuits FUT8-ABA and B4GALT1-ABA that use an abscisic acid (ABA)-inducible system where the presence of ABA triggers the reversible dimerization of the PYL1 and ABI domains. This allows for a PYL1-fused VP16 transcriptional activation domain to be inducibly recruited to a DNA-binding domain based on the PhlF repressor, a homolog of the Tet repressor, linked to ABI.[36] To reduce

185 the likelihood of spurious activation of the PhlF activatable-promoter, a nuclear export signal
186 (NES) was included between the PhlF DNA-binding domain and ABI. A nuclear localization
187 signal (NLS) attached to VP16-PYL1 enables dimerized PhlF-NES-ABI and NLS-VP16-PYL1
188 to enter the nucleus (Fig. 4d). This system exhibits low background activation and high maximal
189 expression levels upon activation.[37] ABA-inducible circuits regulating *FUT8* and *β4GALT1*
190 expression were integrated into LP20 in the *FUT8*$^{-/-}$ or *β4GALT1*$^{-/-}$ cell lines. With circuit FUT8-
191 ABA, 2.8% to 83.4% mAb fucosylation was achieved using increasing ABA concentrations (0-
192 250 uM ABA) (Fig. 4e, Table 1). With circuit B4GALT1-ABA, 1.7% to 76.2% total
193 galactosylation of mAb was achieved using ABA titration (Fig. 4f, Table 1). The highest
194 fucosylation and galactosylation levels achieved in this experiment were slightly lower than
195 those observed with the Dox-inducible systems, and the uninduced levels of fucosylation and
196 galactosylation were lower in the ABA-inducible system. Therefore, the ABA-inducible system
197 has the advantage of tighter control of the uninduced state, and the Dox-inducible system has the
198 benefit of a stronger induced state. Since afucosylated and highly galactosylated/sialylated mAbs
199 are useful for cellular effector function studies, the ABA-inducible system is appropriate for
200 *FUT8* modulation and the Dox-inducible system is best for *β4GALT1* modulation.
201
202 *FUT8 and β4GALT1 genes are independently regulated under inducible promoters*
203 After demonstrating independent control of fucosylation and galactosylation in single
204 knockout clones, we aimed to demonstrate simultaneous independent regulation of both genes in
205 order to produce a mAb with any desired level of fucosylation and galactosylation. Simultaneous
206 and orthogonal control of *FUT8* and *β4GALT1* expression was achieved through integration of
207 circuit FUT8-ABA into LP20 and circuit B4GALT1-Dox into LP8 of the *FUT8*$^{-/-}$/*β4GALT1*$^{-/-}$

208 triple LP cell line (Fig. 5). Circuit FUT8-ABA was chosen for *FUT8* expression due to the tight
209 regulation of the uninduced state of fucosylation using the ABA-inducible system. While
210 complete afucosylation was easily achievable with the deletion of endogenous *FUT8* gene, it was
211 important that the lower range of total fucosylation be accessible for broad effector function
212 modulation, since this has not been rigorously studied.[22,38] Circuit B4GALT1-Dox was chosen
213 for *β4GALT1* expression due to the higher levels of galactosylation using Dox-inducible system,
214 desirable for efficient effector function CDC activity and also required for subsequent
215 sialylation.

216 A range of fucosylation levels from 0.6% to 88.4% was achieved using ABA induction,
217 when total galactosylation was kept at very low levels in the absence of Dox (Fig. 5a, Table 2).
218 At high levels of galactosylation, fucosylation ranged from 1.1% to 83.1%. At very low levels of
219 fucosylation, in the absence of ABA, a range from 3.3% to 74.0% total galactosylation was
220 achieved (Fig. 5b). At high levels of fucosylation, total galactosylation ranged from 2.1% to
221 59.0%. Interestingly, at intermediate levels of fucosylation, total galactosylation ranged from
222 3.8% to 78.8%, which is higher than the ranges observed at low or high fucosylation levels.
223 Fucsosylation and galactosylation appear to have some influence on one another and on
224 mannosylation levels, but further studies are needed to understand these effects. The dual
225 inducible expression systems allow simultaneous and orthogonal control of fucosylation and
226 galactosylation, resulting in a broad range of glycosylated and fucosylated recombinant mAb
227 variants in a precise and tunable manner.

228

229 *Fucosylation and galactosylation levels affect mAb binding affinity to Fc receptor*

With our new ability to control independently both fucosylation and galactosylation levels, we generated mAb variants with nine different glycosylation profiles to test whether these differences affect effector function activity (Fig. 5c). Typical mAbs expressed in CHO cells have high fucosylation levels and low galactosylation levels (Table 1), with both types of modifications influencing antibody effector functions.[8–10,39] ADCC, one of the major effector functions of therapeutic antibodies, is initiated by binding of IgG Fab domain to the target antigen on target cells and IgG Fc domain to FcγRIIIa on the surface of effector cells. The glycosylation profile of the IgG can impact binding of the IgG to FcγRIIIa, which can in turn be determined by surface plasmon resonance (SPR) analysis. Nine different glycosylation variants of mAb, representing various combinations of fucosylation and galactosylation levels (high, medium, and low) were generated by inducing variable *FUT8* and *β4GALT1* expression from circuits FUT8-ABA and B4GALT1-Dox in the *FUT8*$^{-/-}$/*β4GALT1*$^{-/-}$ cell line. The binding affinities of these nine antibody glycoforms to FcγRIIIa were then analyzed by SPR (Fig. 5d, Table 2, Supplementary Fig. 3, Supplementary Table 3). The lowest binding affinity (K_D = 77.9 nM) was observed for mAb variants with 88.4% fucosylation and 2.1% galactosylation. The highest binding affinity (K_D = 8.1 nM) was observed for mAb variants with 1.1% fucosylation and 74.0% galactosylation. There was a clear relationship between Fc fucosylation and FcγRIIIa binding, where lower fucosylation levels increased the binding affinity of Fc to FcγRIIIa. In addition, higher Fc galactosylation levels resulted in increased binding affinity. Our statistical analyses indicate that fucosylation, and to a lower extent galactosylation, affect binding (Supplementary Fig. 4). These data are in good agreement with previous studies showing negative and positive correlation of binding affinities with fucosylation and galactosylation

252 levels, respectively.[39,40] Other potentially important glycan structures for binding are reported in
253 the Supplementary Fig. 4b.
254
255 **Discussion**
256 In this work, we precisely tuned antibody fucosylation and galactosylation levels by
257 knocking out endogenous *FUT8* and *β4GALT1* genes and then demonstrating precise control of
258 exogenous *FUT8* and *β4GALT1* gene expression under small molecule inducible promoters.
259 Expression from endogenous *FUT8* and *β4GALT1* genes results in mAb exhibiting high
260 fucosylation, low galactosylation, and even lower sialylation. When expressed with controllable
261 levels of *FUT8* and *β4GALT1* genes, mAb fucosylation levels range from 0.3% up to 91.5%,
262 while galactosylation levels range from 1.9% to as high as 80.8%. While there has been some
263 progress in engineering the expression host or enzymatically modifying purified mAbs, we have
264 engineered cells with synthetic gene circuits integrated into the genome to stably express these
265 glycosyltransferase genes at tunable levels, allowing for a wide range of galactosylated and
266 fucosylated species not easily accessible before. Achieving high galactosylation levels and
267 concomitant higher sialylation levels is promising for a field hampered by the difficulty of
268 generating products with suitable sialylation levels for clinical use.
269 The Dox and ABA inducible systems are powerful, but some adaptation is required
270 before these systems could be used industrially. Inducible synthetic circuits are exciting in this
271 regard because the integration of one circuit in a knockout cell line allows for the realization of
272 an entire range of glycosylation levels, while other host engineering approaches require the
273 development of a new cell line for each new glycosylation target. However, the use of small
274 molecule inducers during mAb production may be prohibitively costly as they must be removed

during purification then properly disposed. To circumvent this issue, the system could be adapted to use a photo- or temperature-inducible system that could temporally induce gene expression without the addition of small molecules. Alternatively, the small molecule based systems could be used in the research and discovery stage of mAb development to ascertain desirable glycosylation levels, and then a constitutive expression system that maps to the appropriate levels could be used for production at clinical manufacturing stages. Varied glycosylation profiles can result for different protein products even if the same process and cell line host are used, so each new mAb would first require tuning of the glycosylation levels with small molecules before moving to the appropriate constitutive promoters that provides the ideal glycan profile. Nevertheless, the power of simultaneous, precise modulation of each gene means mAbs can now be engineered with specific glycosylation patterns suited for particular Fc-mediated effector functions or to produce biopharmaceuticals with desirable levels of fucosylation and galactosylation. This would be especially valuable for the production of biotherapeutics with unique glycoforms.[4] Additionally, the tools developed here would aid in generating mAb therapeutics with a reproducible glycosylation profile, which is required for safety, efficacy, and regulatory clearance. In the case where only a specific mAb glycoform is biologically active, we can now enrich for the desired glycoform.

The approach used here could be further extended to other glycosyltransferase genes. Now that high levels of galactosylation can be reliably achieved, control of sialylation is the next obvious target, as low galactosylation levels often limit sialylation. As new mAb therapeutics are developed with desirable potency, safety, immunogenicity, and pharmacokinetic properties in mind, the ability to control glycoforms more readily should enable the development of mAbs with such properties. While we used a test mAb, this system should be compatible with all types

of mAbs, including antibody-drug conjugates, mAb fusion proteins, and bispecific monoclonal antibodies. Importantly, this method should be broadly applicable beyond mAb therapeutics to any new recombinant protein therapeutics where precision in N-glycosylation is required for a desired biological effect. Furthermore, this technology could be used to modulate other post-translational modifications, such as O-linked glycosylation, lipid acylation, and phosphorylation, a first step towards the rational engineering of metabolic pathways.

Methods

Landing pad vector construction

Landing pad donor vectors for CRISPR-Cas9 integration in LP2, LP8 and LP20 loci were constructed as described.[26] Briefly, homology arm sequences (typically ~0.5-1 kb long) were synthesized as a single gBlock (Integrated DNA Technologies) containing a PmeI restriction site between the left (LHA) and right (RHA) homology arms, and BsaI cleavage sites in 5' and 3' termini for Golden Gate cloning.[41] Each gBlock was cloned into a pIDTsmart vector (Integrated DNA Technologies) modified to contain compatible BsaI cloning sites. Landing pad cassette 1, containing hEF1a-attP-BxB1-EYFP-P2A-Hygro was constructed using Gateway cloning as previously described.[31,42] LP cassette 2, containing hEF1a-attP-BxB1-GA-EYFP-P2A-Hygro was constructed from LP cassette 1 using PCR mutagenesis. LP cassette 3, containing hEF1a-attP-BxB1-EBFP-P2A-Bla was constructed from LP cassette 1 using in-fusion cloning (Clontech). Landing pad cassettes were cloned into a PmeI linearized pIDTsmart backbones between the left and right homology arms using in-fusion. This resulted in the following donor vectors: LP2-cassette 3, LP8-cassette 3 and LP20-cassette 2 (Supplememtary Fig. 1).

The DNA payload encoding two copies of human monoclonal antibody, called mAb (IgG1 from Pfizer), was constructed using modular Gateway/Gibson assembly as described.[26] Briefly, mAb light chain (LC) and heavy chain (HC) entry vectors were recombined with CMV and hEF1a entry vectors, respectively, and different position vectors to generate CMV-LC and hEF1a-HC expression vectors. Gibson reactions were performed using the Gibson Assembly Ultra Kit (SGI-DNA) using equimolar concentrations (~40 fmols per 10 µL reaction) of column-purified expression vectors, adaptor vector and carrier vector cleaved with I-SceI, XbaI and XhoI and FseI, respectively. Gibson reactions were transformed into *E. cloni* 10G electrocompetent cells (Lucigen) and grown at 30°C in LB media supplemented with ampicillin (100 µg/mL) and kanamycin (50 µg/mL). The resulting attB-BxB1-puro-2x-hEF1a-LC-CMV-HC construct was verified by restriction mapping analysis and sequencing, and expanded in Stbl3 cells (Invitrogen).

Landing pad construction

Single- and multi-LP cell lines in LP2, LP8 and LP20 loci were constructed by homologous recombination with CRISPR/Cas9 as described[26] with the following changes. Targeted integrations were performed by co-transfecting 500 ng of circular LP donor vector with 40 ng of pSpCas9(BB) (pX330) plasmid and 150 ng of U6-gRNA GeneArt DNA String (Thermo). About 10^5 cells were transfected in triplicate with a Neon electroporator (Invitrogen) using 10 pulses of 1560 V and 5 ms width, and seeded in 24-well plate. Three days post-transfection cells were combined and transferred to a 125 mL flask with 10 mL CD-CHO media, recovered for 1 day, and on day 4 subjected to antibiotic selection with either hygromycin (200 µg/mL) or blasticidin (2-20 µg/mL) for two weeks followed by clonal sorting with FACS. Clonal cells were verified

with diagnostic PCR using locus-specific and LP-specific primers (on-target integration) and backbone-specific primers (off-target integration). Clones exhibiting locus-specific and backbone-free integration, and stable and homogenous LP expression were isolated and subsequently used for mAb payload and genetic circuits integrations. pX330-U6-Chimeric_BB-CBh-hSPCas9 was a gift from Feng Zhang (Addgene plasmid # 42230).[43]

CHO cell culture and transfections

Serum-free, suspension adapted CHO-K1 cells (CHO-SF) were grown in CD-CHO media (Gibco), supplemented with 8 mM L-glutamine (Gibco), at 37°C and 7% CO_2 in flasks with shaking at 130 rpm. Seeding density was $3x10^5$ cells/mL and cultures were split every 3 or 4 days. Transfections were always carried out using Neon transfection system (Thermo) at the setting of 1600 V, 10 ms, and 3 pulses with $3x10^5$ cells per 10 μL transfection.

Flow cytometry and single-cell cloning

Cells were analyzed with LSRFortessa flow cytometer, equipped with 405, 488 and 561 nm lasers (BD Biosciences). 30,000 events were collected for analysis, using 488 nm laser and 530/30 nm bandpass filter for EYFP and 405 nm laser, 450/50 filter for EBFP. Cell sorting was performed on FACSAria cell sorter. Untransfected CHO-SF cells were used for gate setting. After landing pad integration, EYFP and EBFP positive cells were sorted into 96-well plates. After mAb circuit or synthetic gene circuit integration, different selection and sorting schemes were applied to select payload integrants based on the loss of EBFP or gain of mKate signal. Single cells were sorted into 96-well plates, and expanded to 24-well and then 6-well plates.

Generation of knockout cell lines and genomic PCR diagnostic test

Cells were transfected with 250 ng U6-gRNA GeneArt DNA String (Thermo) pairs (Supplementary Table 1) and 250 ng pSPCas9(BB)-2A-GFP (PX458) into dLP cells with mAb integrated into LP2. Three days post transfection, cells were sorted for GFP-positive single cells and genomic DNA was assayed by PCR for exon excision (Supplementary Table 2). pSPCas9(BB)-2A-GFP (PX458) was a gift from Feng Zhang (Addgene plasmid # 48138).[44]

Construction and integration of genetic circuits

A synthetic *FUT8* gene (cDNA sequence comprising 11 exons) and a synthetic *β4GALT1* gene (cDNA sequence comprising 5 exons) were acquired as gBlocks from IDT. Each gBlock included a Kozak sequence upstream of the cDNA sequence. Modular Gateway/Gibson assembly (SGI-DNA) was used in the construction of all genetic circuits (Supplementary Fig. 5).[10] Circuit integration requires transfection of 500 ng pEXPR-BxB1 and at least 500 ng of each circuit. Three days post transfection, mKate signal was assayed by FACS analysis. Selection may be carried out for 7 days (200 μg/mL hygromycin or 20 μg/mL blasticidin). Ten days post transfection, cells were sorted for mKate-positive and EYFP-negative cells (circuit integration into LP20 locus) or for mKate-positive and EBFP-negative cells (circuit integration into LP8 locus). SV-ABAactDA was a gift from Jerry Crabtree (Addgene plasmid # 38247).[37]

Fed-batch culture and glycan analysis

Seven-day fed batch cultures, with three biological replicates of each condition (25 mL in 125 mL shake flasks), were seeded at 1.5×10^6 cells/mL in CD-CHO media supplemented with 8 mM L-glutamine. On days 3 through 6, cultures were titrated to pH 7.2 twice a day with 0.94 M

390 Na_2CO_3/0.06 M K_2CO_3. On and day 3, cultures were supplemented with 0.5 mL of HyClone Cell
391 Boost 5 Supplement (GE Healthcare) and 100 µL 20% (w/v) D-glucose. On days 4 through 6,
392 cultures were supplemented with 1 mL of HyClone Cell Boost 5 and 200 µL 20% (w/v) D-
393 glucose. When required to induce expression of synthetic circuits, doxycycline hyclate (Sigma)
394 was added every 48 hours or (±)-abscisic acid (Sigma) was added every 24 hours to the fed batch
395 culture starting on day 0. 100 µM and 1 mM Dox solutions were made in water. 50 mM ABA
396 stocks were made in ethanol and 250 mM ABA stocks were made as a suspension in 1%
397 hydroxypropyl methylcellulose (HPMC). Cultures were harvested on day 7 and the clarified
398 media (5000 x g, 5 min) was saved for titer measurement by Octet with ProA biosensors (Pall
399 ForteBio) and for mAb purification on ProA resin. Glycans were enzymatically cleaved off of
400 purified mAb, derivatized with 2-aminobenzamide labeling agent, and analyzed by HILIC.[45] A
401 Waters HPLC instrument was used for HILIC with a Waters XBridge Amide column (3.5 µm,
402 4.6 x 150 mm).
403
404 *FcγRIIIa binding SPR analysis*
405 A Biacore™ T200 instrument (GE Healthcare) with Control Software version 2.0.1 and
406 Evaluation software version 3.0 was used for interaction analysis. Anti-PENTA Histidine mAb
407 (Qiagen) diluted in 10 mM sodium acetate (pH 4.5) at 10 µg/mL was directly immobilized
408 across a Series S CM5 biosensor chip (GE Healthcare) using a standard amine coupling kit
409 according to manufacturer's instructions. Un-reacted moieties on the biosensor surface were
410 blocked with ethanolamine. Anti-PENTA Histidine mAb immobilization procedure yielded
411 approximately 1500 RU surface density. Modified carboxymethyl dextran surface containing
412 captured Fcγ receptor via immobilized anti-PENTA Histidine mAb across flow cells 2 and 4

were used as a reaction surface. A similar modified carboxymethyl dextran surface without Fcγ receptors across flow cells 1 and 3 were used as a reference surface. Recombinant human FcγRIIIa-158V (ligand) expressed in Human Embyronic Kidney 293 (HEK293) cells was purchased from Syngene. All mAbs were purified over ProA resin and then dialyzed into PBS. Finally, all the purified mAbs were aliquoted and stored at 10 °C until used for kinetic assay.

For the FcγRIIIa-158V capture assay, the sample compartment of the Biacore T200 system was set to 10 °C, the analysis temperature to 25 °C and the data collection rate to 1 Hz. HBS-EP+ was used as running buffer. In each cycle FcγRIIIa-158V (ligand) at 1 µg/mL in HBS-EP+ was injected for 60 seconds at a flow rate of 50 µl/min, to reach minimum capture levels of around 50 RU. mAb antibody, 4.7 to 150.4 µg/mL in HBS-EP+, was injected for 180 seconds followed by a dissociation phase of 300 s for all six antigen concentrations and the surface was regenerated with 10 mM Glycine pH 1.5 solution per kit instructions (300 s contact). The association and dissociation rate constants, k_a (unit $M^{-1}s^{-1}$) and k_d (unit s^{-1}) were determined under a continuous flow rate of 50 µl/min.

The binding data were initially processed using the Evaluation version 3.0 software. The double reference subtracted data generated using FcγRIIIa-158V capture assay was globally fitted to a 1:1 Langmuir binding model. Rate constants for the mAb-FcγRIIIa-158V interactions were derived by making kinetic binding measurements at six different analyte concentrations ranging from 31.25 – 1000 nM. Association and dissociation rate constants were extracted from binding data using global fit analysis (allowing identical values for each curve in the data set). The R_{max} parameter setting was floated fit locally. The equilibrium dissociation constant (unit M) of the reaction between Fcγ receptor and mAbs was then calculated from the kinetic rate

constants by the following formula: $K_D = k_d / k_a$. For each biological sample, the K_D was determined from one or two technical replicates.

458 **Table captions**

459 Table 1 – Glycosylation profiles for mAb expressed in WT CHO cells; *FUT8*$^{-/-}$ cells; *β4GALT1*$^{-/-}$

460 cells; *FUT8*$^{-/-}$ cells integrated with FUT8-C, FUT8-Dox, or FUT8-ABA circuits; *β4GALT1*$^{-/-}$

461 cells integrated with B4GALT1-C, B4GALT1-Dox, or B4GALT1-ABA circuits; and *FUT8*$^{-/-}$

462 /*β4GALT1*$^{-/-}$ cells integrated with FUT8-ABA and B4GALT1-Dox circuits. The ranges indicate

463 the lowest and highest levels achieved with small molecule inducers.

464

Sample Name	Fucosylated (%)	High Mannose (%)	Sialylated (%)	Terminal Galactosylated (%)	Total Galactosylated (%)
mAb WT	88.8	1.5	0.0	9.5	9.5
FUT8$^{-/-}$	0.3	1.9	0.0	14.9	14.9
β4GALT1$^{-/-}$	90.8	1.6	0.3	2.3	2.6
FUT8$^{-/-}$ + FUT8-C	92.7	2.4	0.5	17.3	17.8
β4GALT1$^{-/-}$ + B4GALT1-C	93.5	0.8	6.8	80.3	87.1
FUT8$^{-/-}$ + FUT8-Dox	9.3 – 94.0	1.9 – 3.4	0.1 – 0.5	12.6 – 21.3	12.7 – 21.7
β4GALT1$^{-/-}$ + B4GALT1-Dox	93.5 – 97.3	0.5 – 1.1	0.4 – 4.2	2.3 – 73.9	3.0 – 78.1
FUT8$^{-/-}$ + FUT8-ABA	2.8 – 83.4	1.5 – 5.9	0.2 – 0.4	11.2 – 14.8	11.4 – 15.0
β4GALT1$^{-/-}$ + B4GALT1-ABA	91.0 – 97.2	0.4 – 1.9	0.2 – 2.5	1.3 – 73.8	1.7 – 76.2
FUT8$^{-/-}$/*β4GALT1*$^{-/-}$	0.0	4.9	0.0	0.0	0.0
FUT8$^{-/-}$/*β4GALT1*$^{-/-}$ + FUT8-ABA + B4GALT1-Dox	0.5 – 88.4	1.9 – 6.2	0.0 –3.0	1.2 – 75.8	2.1 – 78.8

465

466

Table 2 – Glycosylation profiles and binding affinity to FcγRIIIa for mAb upon variable induction conditions of FUT8-ABA and B4GALT1-Dox circuits in *FUT8*$^{-/-}$/*β4GALT1*$^{-/-}$ cells. Mean and standard deviation values are from three biological replicates.

Sample Name	K_D (nM)	Fucosylated (%)	Terminal Galactosylated (%)	Total Galactosylated (%)
0 μM ABA, 0 μM Dox	13.6 ± 2.4	0.6 ± 0.3	3.3 ± 0.3	3.3 ± 0.3
20 μM ABA, 0 μM Dox	22.7 ± 5.8	50.5 ± 2.9	3.5 ± 0.4	3.8 ± 0.3
250 μM ABA, 0 μM Dox	77.9 ± 10.9	88.4 ± 2.7	1.2 ± 0.4	2.1 ± 0.1
0 μM ABA, 0.5 μM Dox	10.3 ± 2.6	0.5 ± 0.4	42.7 ± 4.8	43.9 ± 4.3
20 μM ABA, 0.5 μM Dox	13.8 ± 4.5	35.4 ± 8.7	50.3 ± 4.6	52.1 ± 3.9
250 μM ABA, 0.5 μM Dox	61.1 ± 11.9	87.2 ± 2.7	28.3 ± 4.7	29.7 ± 4.7
0 μM ABA, 3 μM Dox	8.1 ± 1.9	1.1 ± 0.1	71.3 ± 2.8	74.0 ± 2.2
20 μM ABA, 3 μM Dox	10.5 ± 2.8	30.1 ± 2.5	75.8 ± 2.4	78.8 ± 1.8
250 μM ABA, 3μM Dox	41.2 ± 9.0	83.1 ± 3.1	56.4 ± 4.0	59.0 ± 3.7

Figure captions

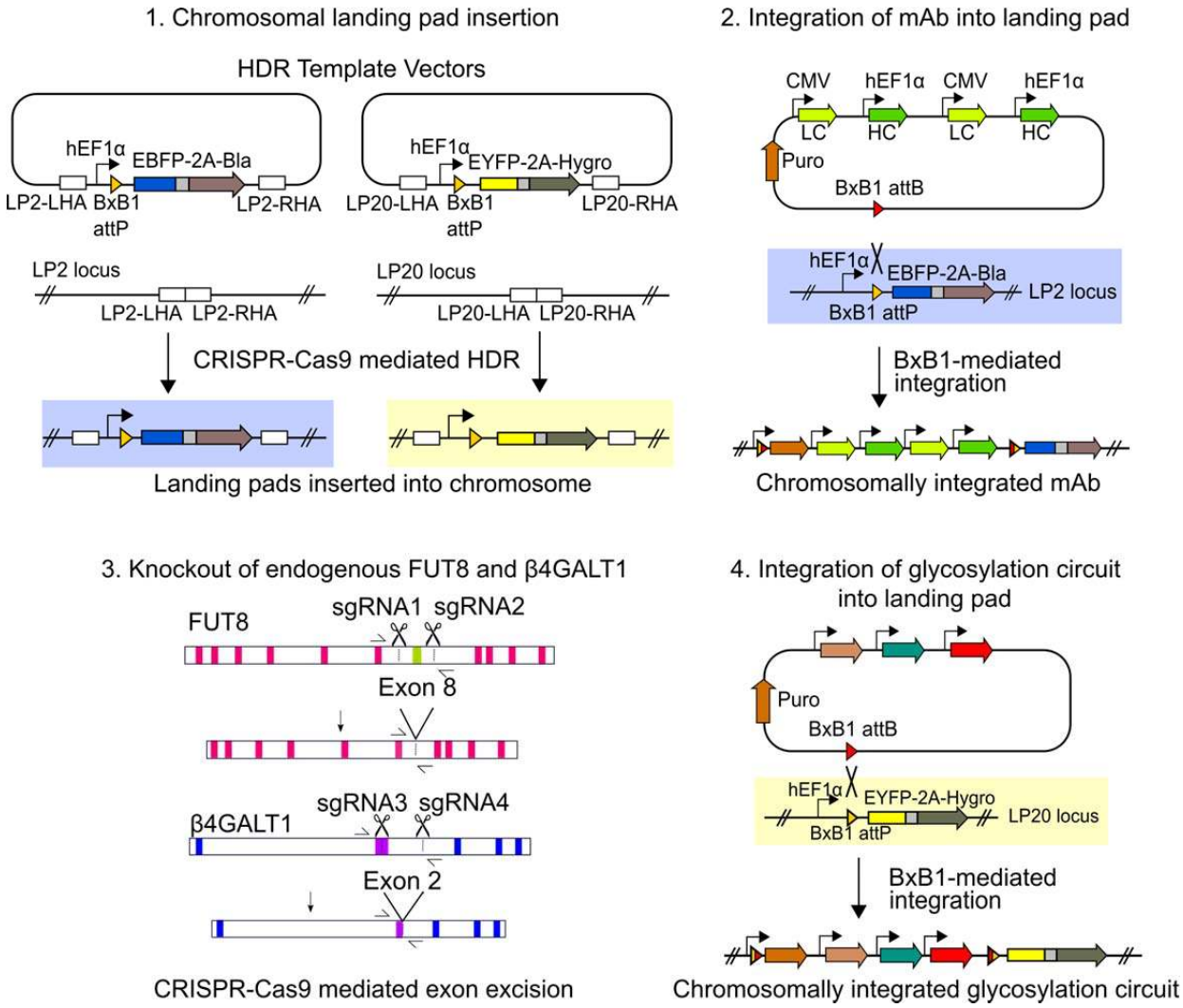

Figure 1 – Overview of cell engineering for mAb and synthetic gene circuits expression in knockout cell lines. CHO cells bearing multiple genomic landing pads were generated using CRISPR/Cas9 mediated homology-directed repair. The LP2 locus was integrated with a payload expressing two copies of mAb light and heavy chains using BxB1 recombinase. Following the integration, LP-mAb integrants were selected with puromycin and verified by cessation of expression of EBFP-2A-Bla cassette. Next, *FUT8* and *β4GALT1* knockouts were generated using CRISPR/Cas9 targeted excision of exons in the catalytic domains. Lastly, the LP20 locus

was integrated with a synthetic gene circuit using BxB1 recombinase. LP-circuit integrants were verified by cessation of expression of EYFP-2A-Hygro cassette.

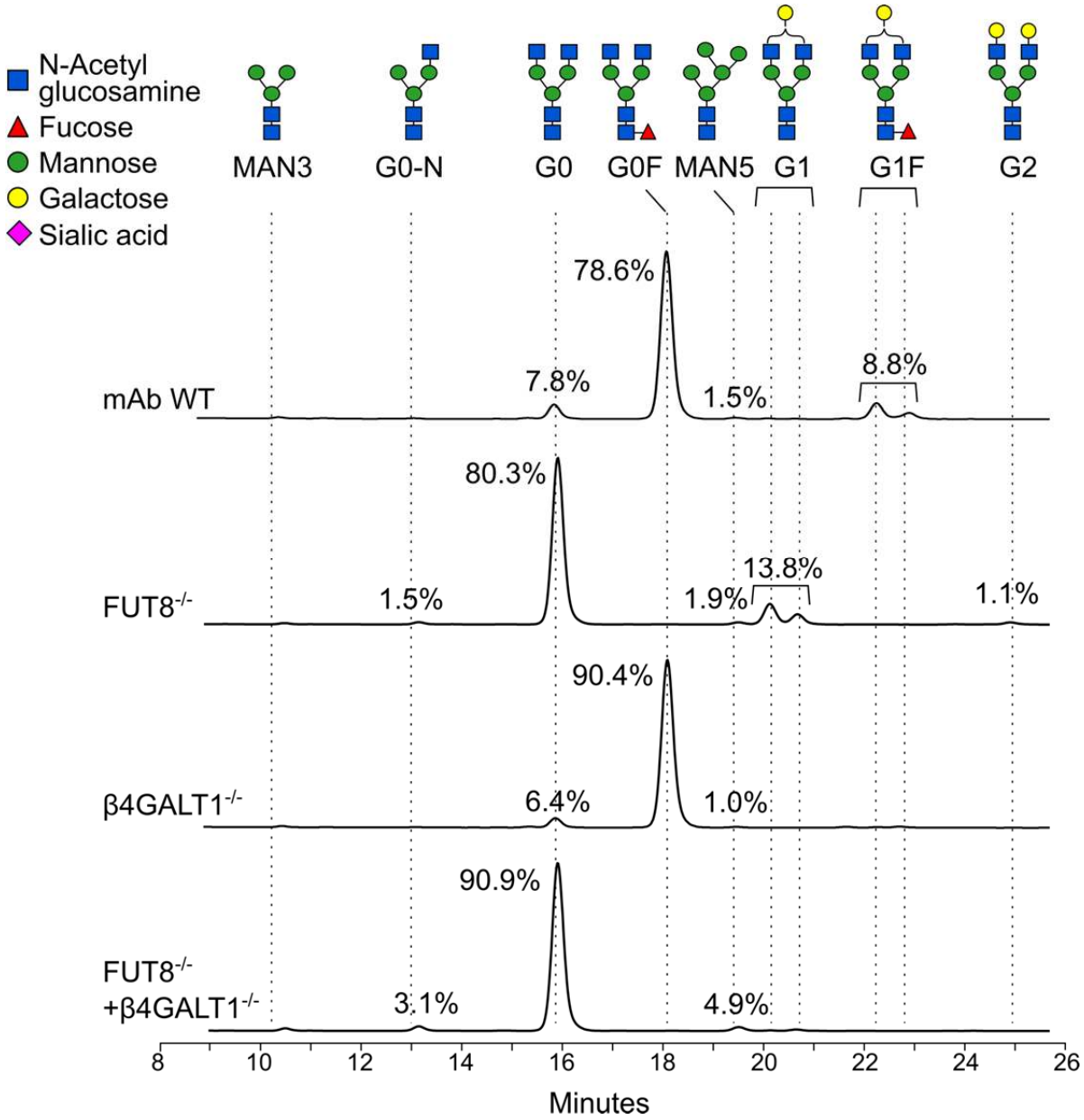

Figure 2 – HILIC analysis shows that *FUT8* and *β4GALT1* gene deletions abolish mAb fucosylation and galactosylation. Symbolic representations of the N-glycan structures are depicted above their corresponding peaks.

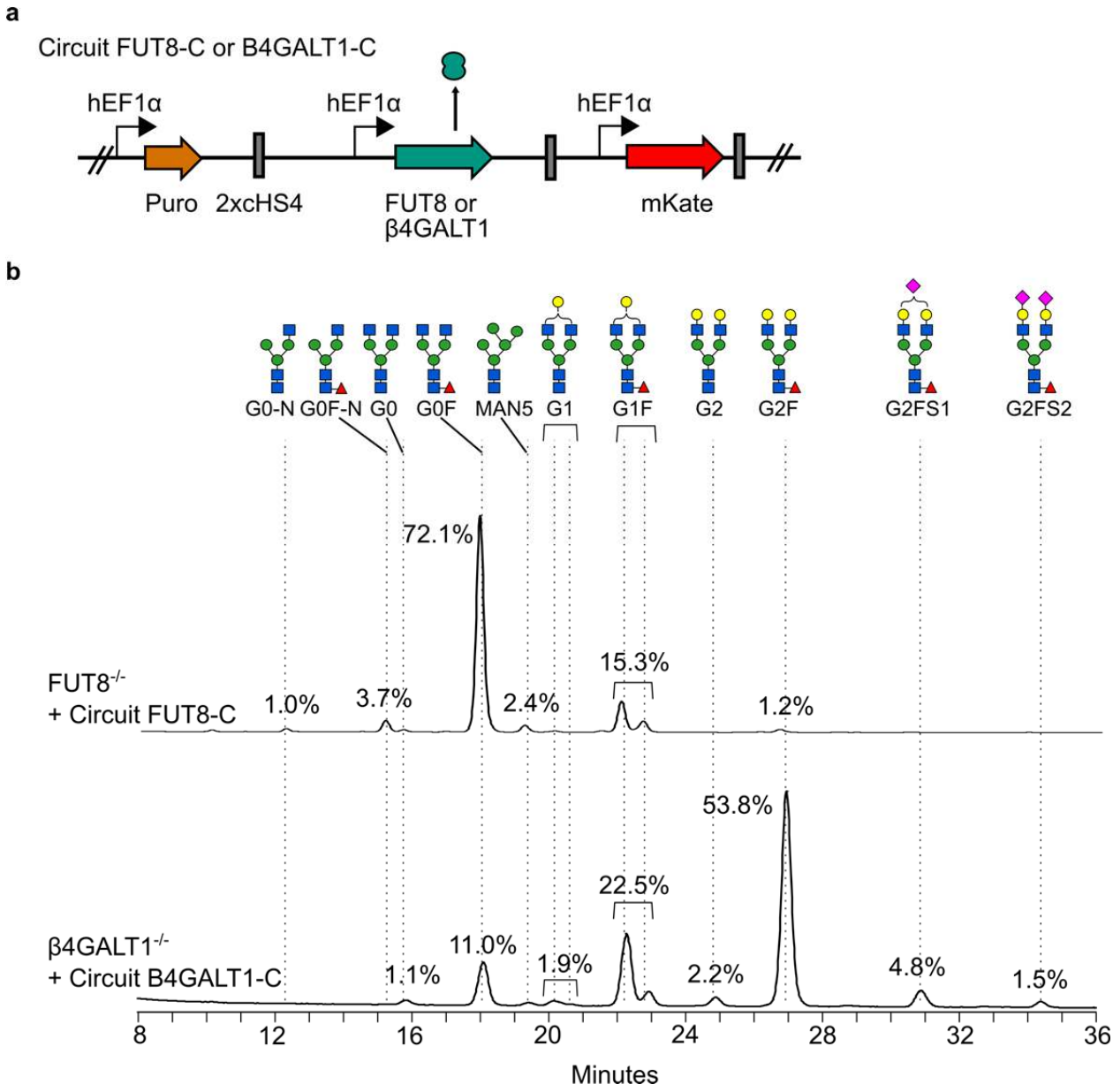

Figure 3 – Circuits constitutively expressing synthetic *FUT8* or *β4GALT1* genes and integrated into engineered cells with the deleted endogenous genes result in highly fucosylated or galactosylated antibody. (a) Circuits FUT8-C and B4GALT1-C express *FUT8* or *β4GALT1* under the constitutive promoter, hEF1a. A puromycin resistance marker and mKate fluorescent marker were used in the selection and sorting of cells integrated into the LP20 of double LP cell line. Two copies of cHS4 insulator sequences separated transcription units. (b) HILIC analysis

503 shows that FUT8-C expression in *FUT8*$^{-/-}$ cells leads to near wild-type levels of fucosylation and
504 slightly increased galactosylation levels. B4GALT1-C expression in *β4GALT1*$^{-/-}$ cells leads to a
505 significant increase in G2F and a 13-fold increase in total galactosylation levels compared to
506 wild-type cells expressing mAb. Symbolic representations of the N-glycan structures are
507 depicted above their corresponding peaks.
508

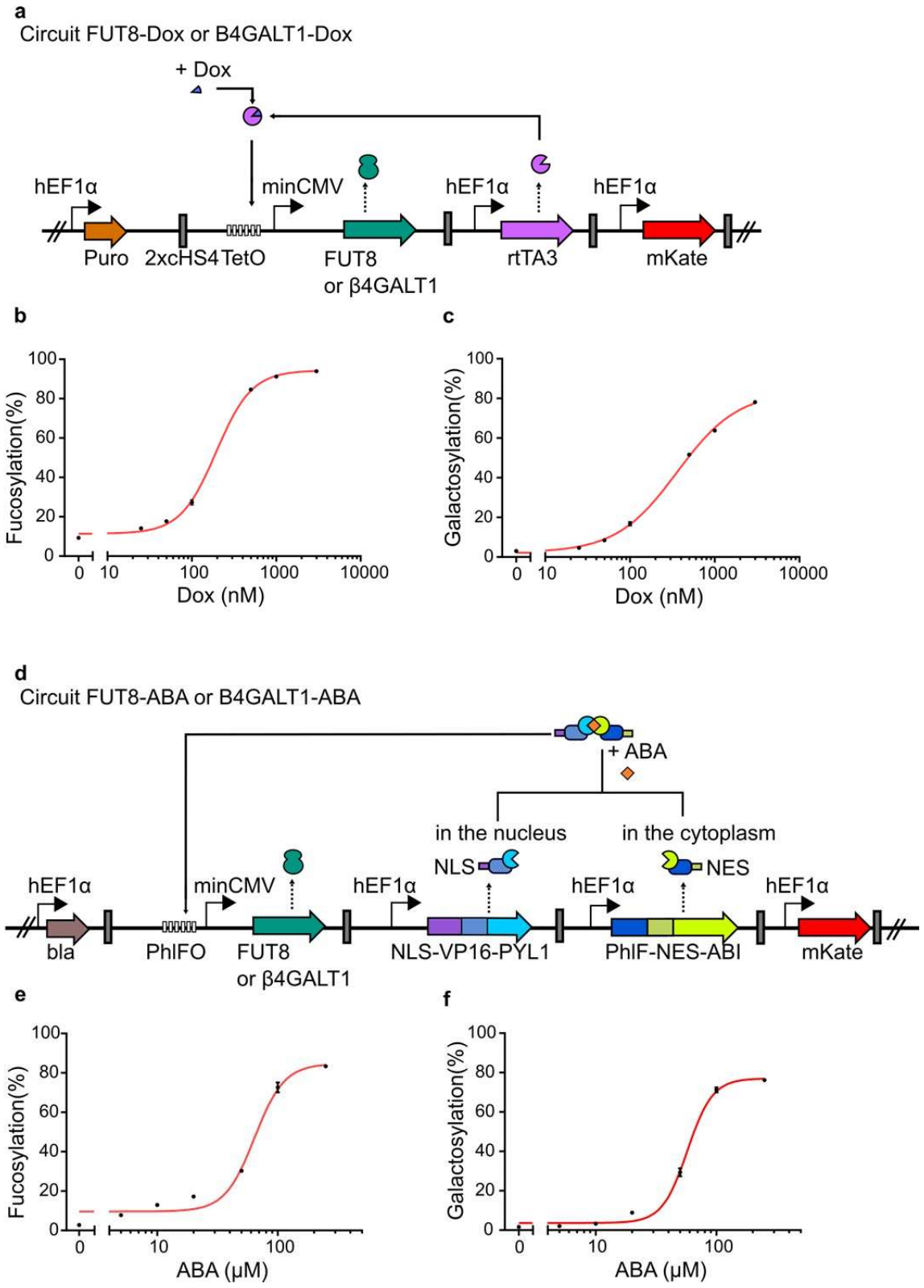

Figure 4 – Gene circuits encoding synthetic *FUT8* or *β4GALT1* genes under small molecule inducible promoters result in the ability to precisely modulate levels of fucosylated or

galactosylated antibody in *FUT8*$^{-/-}$ or *β4GALT1*$^{-/-}$ cells. (a) FUT8-Dox and B4GALT1-Dox circuits express *FUT8* and *β4GALT1* genes under doxycycline-inducible TREt promoter, respectively. Dox binding to rtTA3 induces expression of *FUT8* or *β4GALT1* genes from the TREt promoter, which consists of six TetO sequences upstream of a minimal CMV promoter. Dox dose-dependent activation of *FUT8* or *β4GALT1* expression from FUT8-Dox or B4GALT1-Dox circuits leads to changes in (b) fucosylation or (c) galactosylation. (d) FUT8-ABA and B4GALT1-ABA circuits express *FUT8* and *β4GALT1* genes under an abscisic acid-inducible PhlF-activatable promoter, which consists of six PhlF operators upstream of a minimal CMV promoter. ABA induces dimerization of PYL1 and ABI domains (which are spatially segregated by a nuclear localization signal or a nuclear export signal, respectively), resulting in association of PhlF DNA binding domain and VP16 transcription activation domain, which induces gene expression. ABA dose-dependent activation of *FUT8* or *β4GALT1* expression from FUT8-ABA or B4GALT1-ABA circuits leads to changes in (e) fucosylation or (f) galactosylation. For all plots, data represent the mean and standard deviation (indicated by error bars) of three biological replicates. A red line is included as a visualization guide for the data.

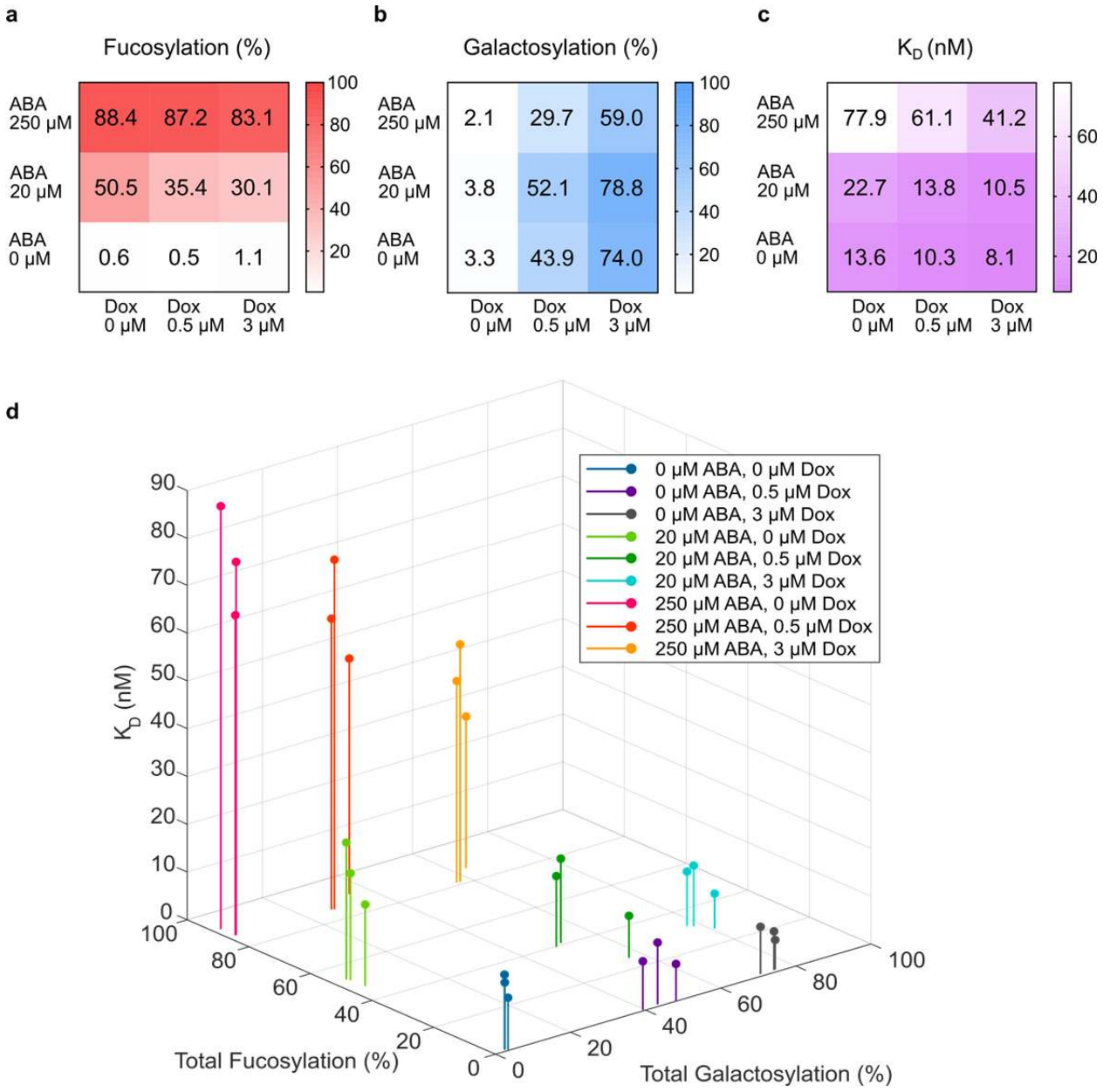

Figure 5 – Simultaneous, independent regulation of *FUT8* and *β4GALT1* gene expression in *FUT8*$^{-/-}$/*β4GALT1*$^{-/-}$ cells integrated with FUT8-ABA circuit in LP20 and B4GALT1-Dox circuit in LP8 led to a wide range of fucosylation and galactosylation levels and various levels of binding affinity of mAb to FcγRIIIa. Heat map representation of (a) fucosylation, (b) galatosylation, and (c) K_D of mAb binding to FcγRIIIa. K_D levels were determined by SPR analysis of FcγRIIIa binding to mAb glycoforms with variable fucosylation and galactosylation

levels. All numbers presented in the heat maps are mean values from three biological replicates. (d) 3D plot correlating mAb fucosylation, galactosylation and binding affinity to FcγRIIIa. Nine mAb glycoforms with combinations of low, medium, and high levels of fucosylation and galactosylation, and their corresponding K_D values for FcγRIIIa binding. Three biological replicates for each condition are represented as individual bars.

References

1. Weiner, L. M., Murray, J. C. & Shuptrine, C. W. Antibody-based immunotherapy of cancer. *Cell* **148,** 1081–4 (2012).
2. Jefferis, R. Recombinant antibody therapeutics: the impact of glycosylation on mechanisms of action. *Trends in Pharmacological Sciences* **30,** 356–362 (2009).
3. Chiu, M. L. & Gilliland, G. L. Engineering antibody therapeutics. *Curr. Opin. Struct. Biol.* **38,** 163–173 (2016).
4. Liu, L. Antibody glycosylation and its impact on the pharmacokinetics and pharmacodynamics of monoclonal antibodies and Fc-fusion proteins. *Journal of Pharmaceutical Sciences* **104,** 1866–1884 (2015).
5. Solá, R. J. & Griebenow, K. A. I. Effects of Glycosylation on the Stability of Protein Pharmaceuticals. *Biochemistry* **98,** 1223–1245 (2010).
6. Arnold, J. N., Wormald, M. R., Sim, R. B., Rudd, P. M. & Dwek, R. A. The Impact of Glycosylation on the Biological Function and Structure of Human Immunoglobulins. *Annu. Rev. Immunol.* **25,** 21–50 (2007).
7. Higel, F., Seidl, A., Sörgel, F. & Friess, W. N-glycosylation heterogeneity and the

influence on structure, function and pharmacokinetics of monoclonal antibodies and Fc fusion proteins. *Eur. J. Pharm. Biopharm.* **100,** 94–100 (2016).

8. Shinkawa, T. *et al.* The absence of fucose but not the presence of galactose or bisecting N-acetylglucosamine of human IgG1 complex-type oligosaccharides shows the critical role of enhancing antibody-dependent cellular cytotoxicity. *J. Biol. Chem.* **278,** 3466–3473 (2003).

9. Reusch, D. & Tejada, M. L. Fc glycans of therapeutic antibodies as critical quality attributes. *Glycobiology* **25,** 1325–1334 (2015).

10. Hodoniczky, J., Yuan, Z. Z. & James, D. C. Control of recombinant monoclonal antibody effector functions by Fc N-glycan remodeling in vitro. *Biotechnol. Prog.* **21,** 1644–1652 (2005).

11. Wang, L. X. & Lomino, J. V. Emerging technologies for making glycan-defined glycoproteins. *ACS Chem. Biol.* **7,** 110–122 (2012).

12. Dekkers, G. *et al.* Multi-level glyco-engineering techniques to generate IgG with defined Fc-glycans. *Sci. Rep.* **6,** 36964 (2016).

13. Tejwani, V., Andersen, M. R., Nam, J. H. & Sharfstein, S. T. Glycoengineering in CHO Cells: Advances in Systems Biology. *Biotechnology Journal* **13,** (2018).

14. Li, F., Vijayasankaran, N., Shen, A. (Yijuan), Kiss, R. & Amanullah, A. Cell culture processes for monoclonal antibody production. *MAbs* **2,** 466–79 (2010).

15. Gramer, M. J. *et al.* Modulation of antibody galactosylation through feeding of uridine, manganese chloride, and galactose. *Biotechnol. Bioeng.* **108,** 1591–1602 (2011).

16. Mori, K. *et al.* Engineering Chinese hamster ovary cells to maximize effector function of produced antibodies using FUT8 siRNA. *Biotechnol. Bioeng.* **88,** 901–908 (2004).

17. Yamane-Ohnuki, N. *et al.* Establishment of FUT8 knockout Chinese hamster ovary cells: An ideal host cell line for producing completely defucosylated antibodies with enhanced antibody-dependent cellular cytotoxicity. *Biotechnol. Bioeng.* **87,** 614–622 (2004).

18. Malphettes, L. *et al.* Highly efficient deletion of FUT8 in CHO cell lines using zinc-finger nucleases yields cells that produce completely nonfucosylated antibodies. *Biotechnol. Bioeng.* **106,** 774–783 (2010).

19. Cristea, S. *et al.* In vivo cleavage of transgene donors promotes nuclease-mediated targeted integration. *Biotechnol. Bioeng.* **110,** 871–880 (2013).

20. Sun, T. *et al.* Functional knockout of FUT8 in Chinese hamster ovary cells using CRISPR/Cas9 to produce a defucosylated antibody. *Eng. Life Sci.* **15,** 660–666 (2015).

21. Kanda, Y. *et al.* Establishment of a GDP-mannose 4,6-dehydratase (GMD) knockout host cell line: A new strategy for generating completely non-fucosylated recombinant therapeutics. *J. Biotechnol.* **130,** 300–310 (2007).

22. Imai-Nishiya, H. *et al.* Double knockdown of alpha1,6-fucosyltransferase (FUT8) and GDP-mannose 4,6-dehydratase (GMD) in antibody-producing cells: a new strategy for generating fully non-fucosylated therapeutic antibodies with enhanced ADCC. *BMC Biotechnol.* (2007). doi:10.1186/1472-6750-7-84

23. Meuris, L. *et al.* GlycoDelete engineering of mammalian cells simplifies N-glycosylation of recombinant proteins. *Nat. Biotechnol.* **32,** 485–489 (2014).

24. Yang, Z. *et al.* Engineered CHO cells for production of diverse, homogeneous glycoproteins. *Nat. Biotechnol.* **33,** 842–844 (2015).

25. Raymond, C. *et al.* Production of α2,6-sialylated IgG1 in CHO cells. *MAbs* **7,** 571–583 (2015).

610 26. Gaidukov, L. *et al.* Multi-landing pad DNA integration platform for mammalian cell
611 engineering. *Nucleic Acids Res.* **46,** 4072–4086 (2018).
612 27. Pilbrough, W., Munro, T. P. & Gray, P. Intraclonal protein expression heterogeneity in
613 recombinant CHO cells. *PLoS One* **4,** (2009).
614 28. Wurm, F. M. Production of recombinant protein therapeutics in cultivated mammalian
615 cells. *Nat. Biotechnol.* **22,** 1393–1398 (2004).
616 29. Du, Z. *et al.* Analysis of heterogeneity and instability of stable mAb-expressing CHO
617 cells. *Biotechnol. Bioprocess Eng.* **18,** 419–429 (2013).
618 30. Lee, J. S., Kallehauge, T. B., Pedersen, L. E. & Kildegaard, H. F. Site-specific integration
619 in CHO cells mediated by CRISPR/Cas9 and homology-directed DNA repair pathway.
620 *Sci. Rep.* **5,** (2015).
621 31. Duportet, X. *et al.* A platform for rapid prototyping of synthetic gene networks in
622 mammalian cells. *Nucleic Acids Res.* **42,** 13440–13451 (2014).
623 32. Zong, H. *et al.* Producing defucosylated antibodies with enhanced in vitro antibody-
624 dependent cellular cytotoxicity via FUT8 knockout CHO-S cells. *Eng. Life Sci.* **17,** 801–
625 808 (2017).
626 33. Kaneko, Y., Nimmerjahn, F. & Ravetch, J. V. Anti-inflammatory activity of
627 immunoglobulin G resulting from Fc sialylation. *Science.* **313,** 670–673 (2006).
628 34. Washburn, N. *et al.* Controlled tetra-Fc sialylation of IVIg results in a drug candidate with
629 consistent enhanced anti-inflammatory activity. *Proc. Natl. Acad. Sci.* **112,** E1297–E1306
630 (2015).
631 35. Dow, L. E. *et al.* Conditional Reverse Tet-Transactivator Mouse Strains for the Efficient
632 Induction of TRE-Regulated Transgenes in Mice. *PLoS One* **9,** e95236 (2014).

633 36. Stanton, B. C. *et al.* Systematic transfer of prokaryotic sensors and circuits to mammalian
634 cells. *ACS Synth. Biol.* **3,** 880–891 (2014).
635 37. Liang, F. Sen, Ho, W. Q. & Crabtree, G. R. Engineering the ABA Plant stress pathway for
636 regulation of induced proximity. *Sci. Signal.* **4,** rs2 (2011).
637 38. Li, T. *et al.* Modulating IgG effector function by Fc glycan engineering. *Proc. Natl. Acad.*
638 *Sci.* **114,** 3485–3490 (2017).
639 39. Thomann, M., Reckermann, K., Reusch, D., Prasser, J. & Tejada, M. L. Fc-galactosylation
640 modulates antibody-dependent cellular cytotoxicity of therapeutic antibodies. *Mol.*
641 *Immunol.* **73,** 69–75 (2016).
642 40. Liu, S. D. *et al.* Afucosylated antibodies increase activation of FcγRIIIa-dependent
643 signaling components to intensify processes promoting ADCC. *Cancer Immunol. Res.* **3,**
644 173–83 (2015).
645 41. Engler, C., Gruetzner, R., Kandzia, R. & Marillonnet, S. Golden gate shuffling: a one-pot
646 DNA shuffling method based on type IIs restriction enzymes. *PLoS One* **4,** e5553 (2009).
647 42. Guye, P., Li, Y., Wroblewska, L., Duportet, X. & Weiss, R. Rapid, modular and reliable
648 construction of complex mammalian gene circuits. *Nucleic Acids Res.* **41,** (2013).
649 43. Cong, L. *et al.* Multiplex Genome Engineering Using CRISPR/Cas Systems. *Science.* **339,**
650 819–823 (2013).
651 44. Ran, F. A. *et al.* Genome engineering using the CRISPR-Cas9 system. *Nat. Protoc.* **8,**
652 2281–2308 (2013).
653 45. Shang, T. Q. *et al.* Development and application of a robust N-glycan profiling method for
654 heightened characterization of monoclonal antibodies and related glycoproteins. *J. Pharm.*
655 *Sci.* **103,** 1967–1978 (2014).

Acknowledgements

We thank Francis Lee for help with PCR analysis; Kalpana Jagtap and Selamawit Mamo for help with mammalian cell culture; and Dr. Brian Teague for critical reading of the manuscript.

Author affiliations

Department of Biological Engineering, Massachusetts Institute of Technology, Cambridge, MA, USA

Michelle M. Chang, Leonid Gaidukov, Giyoung Jung, Wen Allen Tseng, Jonathan L. Lyles, Sepideh Dolatshahi, Douglas A. Lauffenburger, Nevin M. Summers, Timothy K. Lu, Ron Weiss

Cell Line Development, Biotherapeutics Pharmaceutical Sciences, Pfizer Inc., Andover, MA, USA

John J. Scarcelli

Analytical Research and Development, Biotherapeutics Pharmaceutical Sciences, Pfizer Inc., Andover, MA, USA

Richard Cornell, Jeffrey K. Marshall, Paul Sakorafas, An-Hsiang Adam Chu, Kaffa Cote, Boriana Tzvetkova

Culture Process Development, Biotherapeutics Pharmaceutical Sciences, Pfizer Inc., Andover, MA, USA

Madhuresh Sumit, Bhanu Chandra Mulukutla, Bruno Figueroa

Author contributions

M.M.C., L.G., G.J., J.J.S., R.C., J.K.M., B.C.M., B.F., D.A.L., N.M.S., T.K.L., and R.W. conceived and designed the study. M.M.C., L.G., G.J. and W.A.T. designed genetic circuits. M.M.C., L.G., G.J., and J.L.L. constructed genetic circuits. M.M.C., L.G., and G.J. constructed cell lines. M.M.C. and G.J. performed fed batch cultures. A-H.A.C., K.C., B.T., and J.K. performed glycan analysis. S.D., D.A.L. and M.S. conceived and performed computational analysis. P.S. performed SPR analysis. M.M.C., L.G., and G.J. wrote the manuscript. All authors commented and approved the manuscript.

Funding

This work was supported by the PTM Pfizer-MIT collaboration.

Competing interests

The authors declare no competing interests.

Corresponding authors

Correspondence to Ron Weiss (Tel: (617) 253-8966; Email: rweiss@mit.edu)